PERFORMANCE OF THE FERMILAB'S 4.3 MEV ELECTRON COOLER *

A. Shemyakin [#], A. Burov, K. Carlson, M. Hu, T. Kroc, J. Leibfritz, S. Nagaitsev, L.R. Prost,
S. Pruss, G. Saewert, C.W. Schmidt, , M. Sutherland, V.Tupikov, A. Warner
FNAL, Batavia, IL 60510, USA

Abstract

A 4.3 MeV DC electron beam is used to cool longitudinally an antiproton beam in the Fermilab's Recycler ring. Cooling capabilities of the electron beam are characterized by the drag rate that was measured at various conditions. Fitting the results with a formula for non-magnetized cooling gives electron parameters that agree within a factor of 2 with independently measured electron beam properties.

INTRODUCTION

In 2005 an electron cooler was installed and commissioned in a 3.3 km, permanent-magnet Recycler ring to assist in storing and cooling of 8 GeV antiprotons. Since the first demonstration in July 2005 [1], electron cooling is used for storing and preparing antiproton bunches for nearly every Tevatron store. At the same time, significant efforts were put to improve stability of operation and to measure and understand the cooling properties of the electron beam.

ELECTRON BEAM GENERATION

The cooler [2] employs a DC electron beam generated in an electrostatic accelerator, Pelletron [3], operated in the energy- recovery mode. The beam is immersed into a longitudinal magnetic field at the gun and in the cooling section (CS); other parts of the beam line use lumped focusing. The main parameters of the cooler are listed in Table 1.

Table 1: Electron cooler main parameters

Parameter	Symbol	Value	Unit
Electron kinetic energy	E_b	4.34	MeV
Beam current	I_b	0.1-0.5	A
High voltage ripple, rms	δU	250	V
CS length	L	20	m
Solenoid field in CS	B_{cs}	105	G
Beam radius in CS	R_b	3-4.5	mm

The operation of electron beam might be significantly affected by full discharges, when the Pelletron voltage drops to zero in a sub-μs time, and the pressure in one of the acceleration tubes increases by several orders of magnitude. The frequency of the discharges depends, in part, on the amount of beam losses to the tube electrodes. Focusing and steering in the deceleration tube was tuned to minimize changes in the current of the deceleration tube's resistive divider at the expense of a slight increase of total losses (Fig. 1). Together with all previous efforts, described in Ref. [4], it allowed stable operation at I_b=0.5 A. The average frequency of full discharges was

once per two days. After two months of operation at 0.5 A, the frequency of discharges started to increase. Because cooling at a higher current was not beneficial (see below), the operational current was decreased to 0.1 A. The reason for the stability degradation at 0.5 A has not yet been understood.
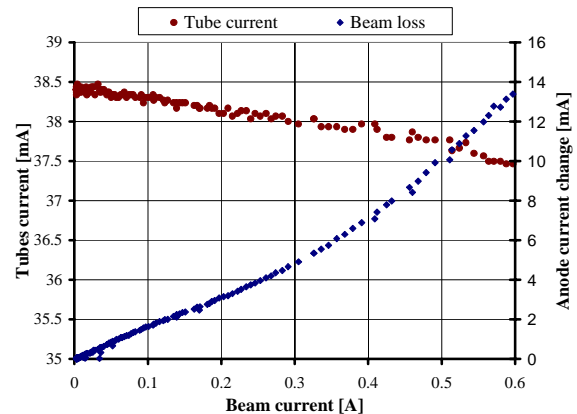

Figure 1: Current losses vs beam current. Blue diamonds are the changes of the anode current, representing the beam current loss. Brown circles are the deceleration tube resistive divider current. The gun voltage is 20 kV.

To estimate ultimate current capabilities of the beam generator, a run in a shorter beam line was performed. In this 12 m line, the beam is turned towards the deceleration tube soon after exiting the acceleration tube. The maximum recorded DC current at E_b = 4.34 MeV was 1.9 A, while 1.6 A was reproducible and stayed up to 10 minutes. Typical relative current losses were 5 ppm at a collector voltage of 3.1 kV and a gun voltage of 40 kV. Further increase of the beam current would require a larger gun voltage and significant modifications to the protection circuitry. Note that demonstration of the same results in the full beam line is more challenging, since the higher electron energy spread [5] and the beam motion caused by the neighboring Main Injector synchrotron's ramping [2] limit the collector efficiency.

ELECTRON BEAM CHARACTERISTICS

The electron beam cooling capability depends on the beam energy spread σ_E, rms value of the electron angles in the cooling section α, and beam current density J_{cs}.

The effective electron energy spread is dominated by the Pelletron HV ripple, δU=250 eV rms. Multiple-coulomb scattering and electron beam density fluctuations [5] are estimated to contribute ~100 eV, added in quadrature.

Table 2 presents estimations of various contributions to the total budget of electron angles. The most uncertain component is the drift velocity. The value in the table is

calculated for the primary beam space charge only, while the effect of slow secondary (ionization) particles would be $\gamma^2 = 100$ times stronger at the same density. To remove ions from the beam, each beam position monitor (BPM) in the cooling section has one of its plates biased to -300 V while the other is grounded. However, it creates potential barriers for secondary electrons, preventing them from leaving the CS along the axis, while the longitudinal magnetic field of the CS prevents them from escaping in the normal direction.

Table 2: Electron angles in CS at $I_b = 0.5$ A. OTR stands for optical transition radiation monitor. Angles are averaged over time, beam cross section, and CS length. The total sums the components in quadrature.

Component	Contribution μrad	Diagnostics
Temperature	70	OTR + pepper pot
Aberrations	50	Simulated
	≤30 @1mm	BPMs
Envelope scalloping	120	Movable orifices
Dipole magnetic field imperfections	40	Magnetic measurements + BPMs
Beam motion	40	BPMs
Drift velocity	20	Calculated
Total	**160**	

One of indications of a possible high density of secondary electrons is the large diameter of a 0.5A, DC electron beam measured in the CS with movable orifices [6]. In these measurements, focusing was adjusted so that the beam envelope oscillations were decreased to < 10%. The spatial period of oscillations of the boundary electrons corresponded to full energy, indicating that they were generated at the cathode. However, the measured beam radius R_b was 4.26 mm, noticeably larger than the radius $R_0 = 3.38$ mm predicted from equality of magnetic fluxes in the cooling section and at the cathode. This increase can be explained by the electric field of secondary electrons with constant density n_2 :and can be expressed as

$$\frac{R_0^2}{R_b^2} = \sqrt{1 - 4\frac{\gamma mc^2}{eB^2 R_b}\cdot(\frac{2I_b}{\gamma^2 \beta c R_b} + 2\pi \cdot n_2 e R_b)} . \quad (1)$$

For the measured radius, Eq. (1) gives the relative density

$$\eta = n_2 (\frac{I_b}{\beta c \pi R^2_b})^{-1} \approx 0.2$$

In this case, the beam rotates with a nearly constant angular velocity, and the electron angle at the boundary is α_{d_max}=0.5 mrad.

Current density in the cooling section J_{cs} can be estimated from the simulated current density J_{cath} at the cathode. If relative variations of the beam radius along the cooling section are low,

$$J_{cs} = J_{cath}(kr) \cdot k^2, \quad (2)$$

where $k=R_{em}/R_b$, and R_{em} is the radius of the emitting surface at a given current. Note that the ratio k can be changed significantly by the presence of secondary electrons.

DRAG RATE MEASUREMENTS

The cooling properties of the electron beam are evaluated in drag rate measurements by a voltage jump method [8]. A low-number (Np=1-5 $\times 10^{10}$), low transverse emittance (ε_t=1-3 π·mm·mrad, 95%, normalized), coasting antiproton beam is electron – cooled to an equilibrium. Then, the electron energy is shifted by a certain value ΔW.
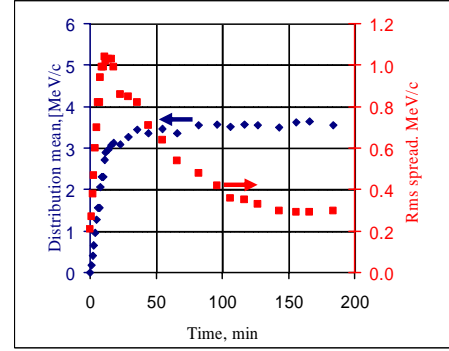

Figure 2: Evolution of the antiproton momentum distribution's average and rms spread after a 2 keV electron energy jump. The measured drag rate is 15 MeV/c per hour. N_p=2.8 $\times 10^{10}$, ε_t=3-6 π mm mrad (n, 95%), I_b= 0.5A. The electron beam was on axis, i.e. was centered with the antiproton beam.

The longitudinal distribution (measured by a Schottky detector) moves, and eventually a new equilibrium is established at a momentum shifted from the initial one by $dP=(M_p/m_e)\Delta W/\beta c$, where M_p and m_e are the proton and electron masses, respectively (Fig.2). The initial time derivative of the average antiproton momentum is taken as a drag rate F.
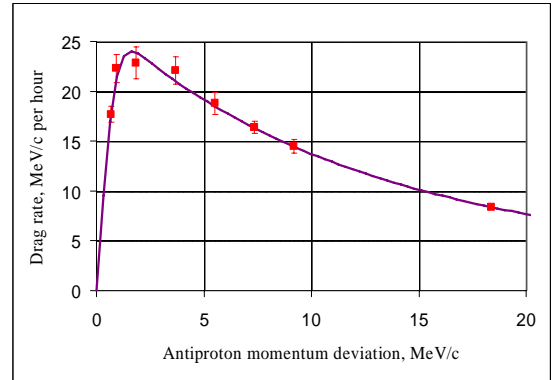

Figure 3: Drag rate as a function of the antiproton momentum deviation. I_b=0.1A, electron beam is on axis. The solid line is a fit by a non-magnetized formula.

The measured dependence F (dP) (Fig.3) fits well with a non-magnetized formula [9] using three fitted parameters of the electron beam: σ_E, α, and J_{cs}. The fitted

values differ from those discussed in the previous section by a factor of 1.5 – 2, depending on the assumed density of secondary electrons. While a statistical error of an individual drag measurement is 2 – 7%, variation in data measured in different days and months was much larger, up to a factor of 2. So far no satisfactory explanation was found.
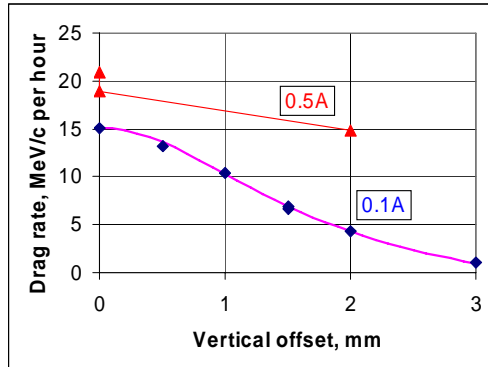

Figure 4: Drag rate as a function of the vertical offset of the electron beam for two beam currents and ΔW=2keV.

The drag force decreases with the vertical offset of the electron beam (Fig. 4). This trend can be caused by decreasing the current density, which is roughly parabolic at I_b= 0.1 A, and by increasing the electron angles towards the beam periphery. If the increase is due to a drift velocity, the total rms angle α is a sum of the drift angle and the rms angle α_0 on the axis, such that

$$\alpha(r)^2 = \alpha_0^2 + \alpha_{d\_max}^2 \cdot (r/R_b)^2 \equiv \alpha_0^2 (1 + (r/b)^2) \cdot$$

Assuming that $F(r) \propto J_{cs}(r)/\alpha(r)^2$, one can fit the experimental data by

$$F(r) = F_0 \frac{1 - (r/a)^2}{1 + (r/b)^2} , \qquad (3)$$

where F_0 is the drag force on axis, and a and b are fitting coefficients describing the radial dependencies of the current density and the rms angle. Fitting with Eq. (3) gives a= 3.5 mm, b=1.7 mm (solid line in Fig.5). These numbers agrees with $J_{cath}(r)$ and Eq. (1) and (2) if one assumes the density of secondary electrons of η= 0.4 and α_0=0.18 mrad.

Measured dependence of the drag rates on the beam current agrees with modeling only within a factor of 2 (Fig. 5). The solid curve follows changes of the simulated current density on axis and is normalized to the most repeatable value for the drag rate at 0.1 A. The maximum recorded drag rate is 37 MeV/c per hour.

Electron cooling is routinely used in operation, and stacks of up to $4 \cdot 10^{12}$ antiprotons were successfully cooled. Comparison of longitudinal cooling rates at various currents shows a trend similar to the one in Fig.5, i.e. the cooling rate is practically constant above 0.1 A. Consequently, recently all cooling is done at 0.1 A with regulation of the cooling rate by a vertical shift of the electron beam. Detailed discussion of operational issues related to electron cooling can be found in Ref.[9].
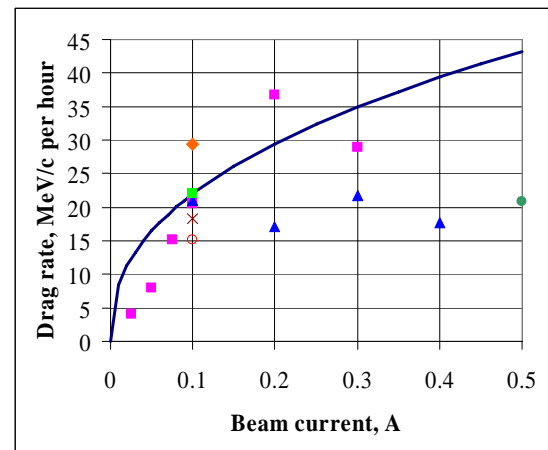

Figure 5: Drag rate as a function of the beam current. Different symbols represent different sets of measurements. The beam is on axis, and ΔW=2keV.

SUMMARY

1. Reliable operation and cooling at DC beam current up to 0.5 A has been demonstrated. The maximum power of a DC beam in a short beam line is 8 MW.
2. Fitting a non-magnetized formula to results of drag rate measurements shows agreement with electron beam parameters within a factor of 2.
3. The major uncertainty in the electron beam parameters might be the density of secondary electrons in the cooling section.

ACKNOWLEDGMENTS

REFERENCES

[1] S. Nagaitsev et al., Phys. Rev. Lett. 96, 044801 (2006).
[2] A. Shemyakin et al., ,AIP Conf. Proc. 821 (2006) 280.
[3] Pelletrons are manufactured by the National Electrostatics Corporation, www.pelletron.com.
[4] L.Prost and A.Shemyakin, AIP Conf. Proc. 821 (2006) 391.
[5] A.Burov et al., AIP Conf. Proc. 821 (2006) 159.
[6] T.K.Kroc et al., AIP Conf. Proc. 821 (2006) 370.
[7] H. Danared et al., Phys. Rev. Lett. 72 (1994) 3775.
[8] Ya.S. Derbenev and A.N. Skrinsky, Particle Accelerators 8 (1977) 1.
[9] L.Prost et al., Electron cooling of 8 GeV antiprotons at Fermilab's Recycler: Results and operational implications, to be published in Proc. of HB2006, Tsukuba, Japan, May 29-June 2, 2006.